# Corrosion resistance of an AlSi alloy (AS12) after sulfuric anodizing and MAO: Mechanisms and effect of sealing with sodium decanoate

Anas Ben Romdhane, Delphine Veys-Renaux, Khaled Elleuch, Emmanuel Rocca

# Corrosion resistance of an Al-Si alloy (AS12) after sulfuric anodizing and MAO: mechanisms and effect of sealing with sodium decanoate

Anas Ben Romdhane[a, b], Delphine Veys-Renaux[a,*],

Khaled Elleuch[b], Emmanuel Rocca [a]

[a] *Université de Lorraine, CNRS, Institut Jean Lamour, F-54000 Nancy, France*

[b] *Laboratoire Génie des Matériaux et Environnement (LGME), ENIS, University of Sfax, BP «1173», 3038 Sfax, Tunisia*

* Corresponding author : delphine.veys-renaux@univ-lorraine.f

**Abstract**

Al-Si alloys, widely used in moulded parts for industrial or domestic applications, may undergo an electrochemical finishing treatment in order to enhance their surface properties, especially their corrosion resistance. In the present study, anodic layers are grown on an AS12 alloy by conventional anodizing in sulfuric acid on the one hand and by microarc oxidation (MAO) on the other hand. While both aluminium and silicon are completely oxidized within the microarc layer, metallic silicon particles are embedded within the classic porous alumina layer formed in acidic medium, generating strains and resulting in a cracked coating. Regarding the corrosion resistance, evaluated comparatively by electrochemical impedance spectroscopy (EIS) measurements performed in NaCl 0.1 M and salt spray test (SST), the results consistently show an improvement by microarc oxidation but not by sulfuric anodizing, since the corrosion mechanisms are mainly driven by galvanic coupling between silicon particles and aluminium matrix. A sealing post-treatment in sodium decanoate $CH_3(CH_2)_8CCONa$ is considered as well on both types of anodic layers. An enhancement of the anticorrosion performances is noticed in each case, more significantly for sulfuric anodizing.

**Keywords :** AS12 alloy ; anodizing ; microarc oxidation (MAO) ; corrosion ; salt spray test (SST) ; electrochemical impedance spectroscopy (EIS)

## 1. Introduction

As Al-Si alloys are known to provide high mechanical strength and good castability, they are materials of choice for moulded parts widely used in various industrial fields such as automotive or household appliances. However, the enhancement of the durability of surfaces subjected to extreme chemical and mechanical stress, requires an additional multifunctional surface treatment. The formation of an oxide in surface may fulfil the expectations and anodizing appears an interesting tool. On the one hand, it is known to improve the corrosion resistance. On the other hand, depending on the anodizing process and mechanism, the morphology (porosity, roughness) may be monitored as well as the physico-chemical nature of the coating, tailoring the hardness and the wear resistance. In acidic medium, anodizing is performed in the voltage range 10 to 30 V and results in the formation of duplex anodic layer made up of an intern barrier layer (about ten nanometres, depending on the voltage) surmounted by a nanoporous alumina network (ten to hundred micrometers depending on the treatment duration) [1-5]. For eco-toxicological reasons, sulfuric acid-based electrolytes are favoured. The presence of alloying elements is known to induce defects in the coatings [6]. Indeed, the literature is rich on acidic anodizing of aluminium alloys with intrinsic high mechanical properties, namely 2XXX and 7XXX alloys. Firstly, the alloying elements in solid solution within aluminium matrix (especially copper) promote water oxidation generating oxygen, a reaction in competition with alumina formation. As consequences, the process efficiency is lowered and the alignment of the nanocolumnar network is modified [7-11]. Furthermore, the presence of secondary intermetallic phases induces the formation of macro-defects in the anodic layer [12-16]. Regarding the Al-Si alloys, the literature is rather poor [17-21] and indicates that the morphology and the physico-chemistry of the anodic layer depends on silicon content and silicon particle size in the substrate. Indeed, silicon may be

present under metallic, partially oxidized or totally oxidized form, which is a key parameter in the further corrosion resistance.

As an alternative to widely used acidic anodizing, the electrochemical conversion may be performed in an alkaline medium. In this case, the passivation range is so broad that the voltage reaches very high values (300 to 500 V), exceeding the dielectric breakdown voltage of the metal/oxide/electrolyte interface [22]. Therefore, the anodizing mechanism turns into a new regime called either “microarc oxidation (MAO)” or “plasma electrolytic oxidation (PEO)” under the effect of sparking discharges [23-24]. Thus, the high temperatures reached in the plasma promote the growth of ceramic oxide phases [25], forming a mesoporous network due to the presence of discharge channels through the coating. The nature of the electrolyte and the electric parameters of the process may be optimized to modulate the porosity and the composition of the coatings, resulting in an enhancement of the corrosion properties [26-29]. As for anodizing in acidic media, microarc oxidation of silicon-containing aluminium alloys has been subject to few investigations [30-33].

As explained above, both the substrate heterogeneities and the anodizing mechanisms may contribute to the formation of morphological defects in the oxide coatings and the post-treatment by a impregnation in a sealing solution is often necessary to improve the anti-corrosion performance [34]. Various components have been identified as an efficient way to clog the porosities and provide anticorrosion protection [35-36], for instance nickel salts [34-37], rare-earth metallic cations [38], silicates [39], fluorometallate salts associated to Cr(III) salts [40-41] or organic compounds [42] and specifically long-chain carboxylate salts [43].

In the present work, the anticorrosion efficiency of coatings elaborated either by sulfuric anodizing or by microarc oxidation on AS12 alloys are evaluated comparatively by Salt Spray Test (SST) and Electrochemical Impedance Spectroscopy (EIS) measurements. The potential enhancement provided by a post-impregnation in a sodium decanoate sealing solution is

assessed as well. The corrosion and protection mechanisms are highlighted based on a fine microscopic and electrochemical description of the anodic layers elaboration and of the coated (and uncoated) materials degradation.

## 2. Materials and methods

*Starting material*

Cast plates (100 mm x 100 mm x 8 mm) of silicon-rich foundry aluminium alloy AS12 were provided by ECAST company (Sfax, Tunisia). The nominal composition was verified locally at some points by optical emission spectrometry and corresponds to the standardized norm of the AS12 alloy given in Table 1. As already described elsewhere [44] (and confirmed by the numerous cross-section observations of the substrate in the present work), the starting alloy mainly consists of an α-aluminium matrix (containing 1.0 ± 0.2 wt.% of silicon) in which pure silicon lamella (length 10–50 μm, width 2–5 μm) are homogeneously dispersed. Intermetallic particles are present as well, containing iron, manganese and silicon ($Al_{15}(Fe,Mn)_3Si_2$ [45]).

**Table 1.** Nominal composition of AS12 alloy (standardized norm)

| Element | Al | Si | Fe | Mn | Cu | Mg | Ni | Zn | Pb | Sn | Ti |
|---|---|---|---|---|---|---|---|---|---|---|---|
| wt.% | 85-86.5 | 12-13 | 0.5-0.8 | 0.3-0.45 | <0.1 | <0.1 | <0.1 | <0.15 | <0.1 | <0.05 | <0.15 |

Samples were prepared by cutting and milling initial plates until 50 mm x 30 mm x 4 mm or 100 mm x 30 mm x 4 mm for further sulfuric anodizing or microarc oxidation respectively. Before surface treatment, the samples were mechanically abraded with SiC papers then polished with a colloidal silica formulation, and finally cleaned with ethanol, rinsed with water and dried with hot air steam.

*Surface treatments*

Sulfuric anodizing was performed in $H_2SO_4$ 1 M, in a 1 L glass beaker in which the sample was connected as an anode (20 $cm^2$ immersed) and placed between two initially etched

titanium cathodes (total of 80 $cm^2$ immersed) with an inter-electrode distance fixed at 4 cm. The temperature was maintained at 23 °C. The experiments were carried out by using a DC power supply from Micronics Systems (max 300 V, 10 A) with an integrated data acquisition system.

Microarc oxidation was performed in an alkaline medium composed of KOH 0.0025 M + $Na_2SiO_3$ 0.01 M + KF 0.001 M. Actually, fluorides and silicates added to the electrolytic bath are known to reinforce the resisting properties of the anodic layer, favouring the initiation of the microarc regime [44]. In a 8 L electrochemical set-up, 45 $cm^2$ of the AS12 sample were immersed between two initially etched titanium electrodes (total area 800 $cm^2$), with an inter-electrode distance fixed at 7 cm. The temperature was maintained around 15 °C thanks to an electrolyte recicrculation system through a plate exchanger cooled by refrigeration unit (Julabo FL4003). The experiments were carried out by using a pulsed power supply from Micronics Systems (max ± 950 V, ± 10 A, 25 Hz). The set-up was connected to a data acquisition system (SEFRAM DAS30) via an amperometric clamp (Chauvin Arnoux E6N CVH1-100) and a differential probe (Elditest GE8115).

For both considered surface treatments, the first experiment consisted in a potentiodynamic scan, performed at 6 V $min^{-1}$ in sulfuric acid and 10 V $min^{-1}$ in the alkaline medium. From these electrochemical investigations, the surface treatment parameters were chosen, namely 15 V in sulfuric acid and a square signal + 100 mA $cm^{-2}$,100 ms / - 100 mA $cm^{-2}$,100 ms for microarc oxidation. After a kinetic study (thickness evaluation by optical microscopy), the duration of both treatments was adjusted in order to get comparable results with a similar anodic layer thickness of 15 µm. The duration of sulfuric anodizing was set at 70 minutes and the duration of microarc oxidation was set at 20 minutes.

The 15 µm thick anodic layers were then impregnated during 30 minutes in a so-called "sealing solution" containing sodium decanoate ($CH_3(CH_2)_8COONa$) with a concentration of

0.01 M. The temperature was fixed to 50°C and the pH to 8.5. Actually, the ten carbons contained in the chain of decanoate are expected to be a good compromise to provide a good corrosion resistance improvement [42-43], while their solubility in the sealing solution has been observed over long periods.

*Morphology and composition characterizations*

Surfaces were investigated by scanning electron microscopy (SEM) (HITACHI S4800 field effect apparatus), by using very low acceleration voltage (1 to 3 kV in order to be sensitive to the extreme surface. The observations were realized after a fine gold plating through round grids serving as masks. The aim of this operation is to ensure a better electrical conductivity of the anodized surfaces while leaving accessible areas with pores not sealed by the metallization. Cross-sections were characterized as well. They were first observed by optical microscopy in order to estimate the average thickness and dispersion around this average thanks to twenty thickness values measured statistically and regularly spaced. Moreover, morphology and composition were in field effect scanning electronic microscope (JEOL J7600F) by combining backscattered electron imagery and energy dispersive X-ray spectrometry (EDS) at an acceleration voltage of 15 kV.

*Corrosion resistance*

Comparative corrosion resistance investigations of the AS12 treated samples and the untreated alloy were performed, using electrochemical methods on the one hand (electrochemical impedance spectroscopy EIS) and non-electrochemical characterizations (salt spray test SST) on the other hand.

EIS measurements were recorded with a Gamry ref 600 potentiostat in a three-electrodes cell in a NaCl 0.1 M corrosive medium. The samples were set horizontally at the bottom of the cell (0.5 $cm^2$), facing to a reference calomel electrode and a platinum grid counter electrode (5

$cm^2$). Electrochemical impedance spectra were recorded after 6 hours of immersion over the frequency range $10^5$ Hz to 5 $10^{-3}$ Hz with 20 mV of amplitude modulation.

SST was performed on large samples (100 mm x 30 mm x 4 mm) in a climatic chamber (VLM CCT 400 FLI) according to the ASTM B117 standard method consisting of a continuous pulverization of a corrosive NaCl 50 g $L^{-1}$ solution at a 35°C fixed temperature. The samples were regularly visually observed and cross section investigations were performed after 240 hours of exposure in a scanning electron microscope (JEOL JSM 6010-LA).

## 3. Results

### *Anodic layers formation and sealing*

The growth of the anodic layers is illustrated in Figures 1-3 in sulfuric medium and Figures 4-6 in alkaline medium. The effect of sealing on both kind of anodic layers is given comparatively on the surface observations, respectively in Figure 3 and 6.

Figure 1 describes the electrochemical behavior of AS12 corresponding to sulfuric anodizing process in $H_2SO_4$ 1 M. The potentiodynamic scan, illustrated in Figure 1a, reveals different steps over the considered range and limits the anodizing voltage at 25 V. Indeed, beyond this threshold, the current density shows a sharp increase, corresponding to water oxidation under the effect of the electric field at this voltage, as already observed [46- 47]. Below the voltage of this dielectric breakthrough, the passivation range seems to be interrupted around 5 V by an anodic peak and may be divided into two passivation stages with a transition around 20 V. If the anodic peak is known to be associated to the dissolution of copper rich intermetallic particles, the electrochemical transition could be linked to the specific passive electrochemical behavior of silicon in sulfuric acid. Considering the overall electrochemical behavior of AS12 (Figure 1a), 15 V was chosen to perform potentiostatic anodizing, in order to favor the oxidation of the copper rich intermetallic particles while avoiding the burning phenomenon

closed to the anodizing range limit . The recorded current density over treatment time is represented in Figure 1b and stabilizes around 5 mA $cm^{-2}$ after only three minutes of treatment, which corroborates the order of magnitude of the current density at 15 V recorded in the potentiodynamic scan (Figure 1a).

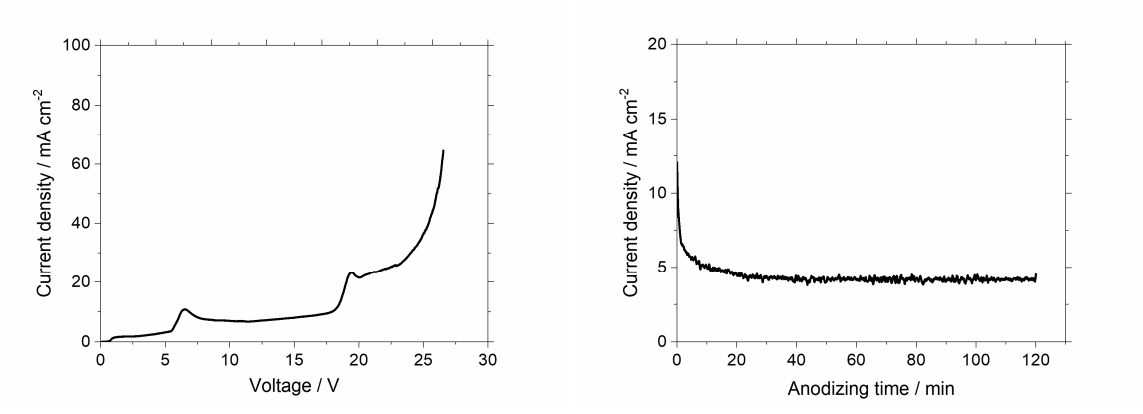


(a) (b)

**Figure 1.** Electrochemical investigation of the sulfuric anodizing process ($H_2SO_4$ 1 M): (a) potentiodynamic scan (6 V $min^{-1}$) over the range 0-27 V; (b) current density over time during an anodizing carried out at 15 V.

The characteristics of the anodic layer grown at 15 V are detailed in Figure 2. Regarding the average thickness, it seems to evolve linearly with anodizing time, as suggested in Figure 2a, with a growth rate around 0.16 µm $min^{-1}$. However, due to the inhomogeneities inside the layer, the thickness exhibits a significant dispersion around the average value. The internal morphology and composition of the layer grown in 90 minutes may be detailed thanks to the SEM cross-section observation depicted in Figure 2b, supplemented by EDX punctual analyses. The anodic layer actually consists of an aluminium oxide matrix, formed over the substrate aluminium matrix, in which the metallic silicon lamella from the substrate are embedded. The Pilling-Bedworth ratio relative to the formation of an anodic layer on an aluminium substrate in the present experimental conditions (electrolyte nature, concentration, temperature, voltage) may be estimated in the range 1.3-1.4 [48]. Therefore, silicon lamella entrapped in the coating induce high stress within the anodic layer which results in horizontal

cracking of these metallic parts. Actually, macro-defects generated in the anodic layers grown on aluminium alloys may result from different phenomena, namely high porosity, dissolution of precipitated intermetallic phases, selective anodizing of aluminium over intermetallic phases, embedding of small size oxidized intermetallic phases within the alumina anodic layer, embedding of metallic or intermetallic phases within the alumina anodic layer, different thermal expansion coefficients in the coating and in the substrate [11-16, 46]. All these configurations may lead to mechanical stress inside the alumina anodic layer and may result in the formation of cracks, with various orientations depending on the macro-defects.

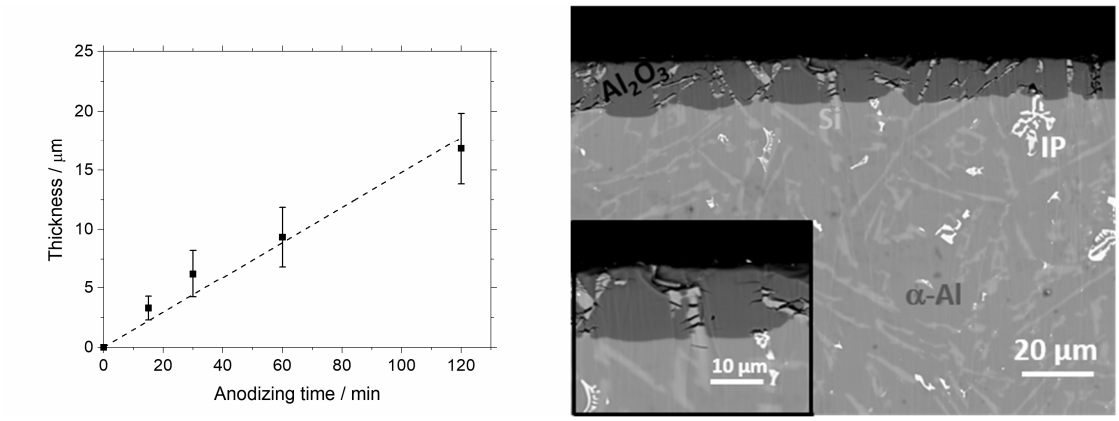


(a) (b)

**Figure 2.** (a) Growth kinetics of the anodic layer in $H_2SO_4$ 1 M at 15 V (average thickness evaluated by optical microscopy); (b) SEM cross-section observation after 90 min of sulfuric anodizing.

As revealed in Figure 3a, the morphology of the anodic layer observed on surface over the α-aluminium matrix (containing 1 wt.% of silicon) is similar to what is usually obtained in $H_2SO_4$ 2M on low alloyed aluminium substrates after anodizing in sulfuric acid [46]. However, the classic alumina nanoporous structure is broken up by through-silicon as shown in Figure 1c, leading to the presence of open spaces between the alumina network and the silicon metallic lamella. The effect of the impregnation in the sealing solution, presented in

Figures 3b and Figure 3d seems to be slight: a very thin, local and partial covering of the alumina nanostructure may be deduced from the observation sensitive to the extreme surface (Figure 3b), and the spaces between the alumina network and the silicon particles seems to be reduced (Figure 3d).

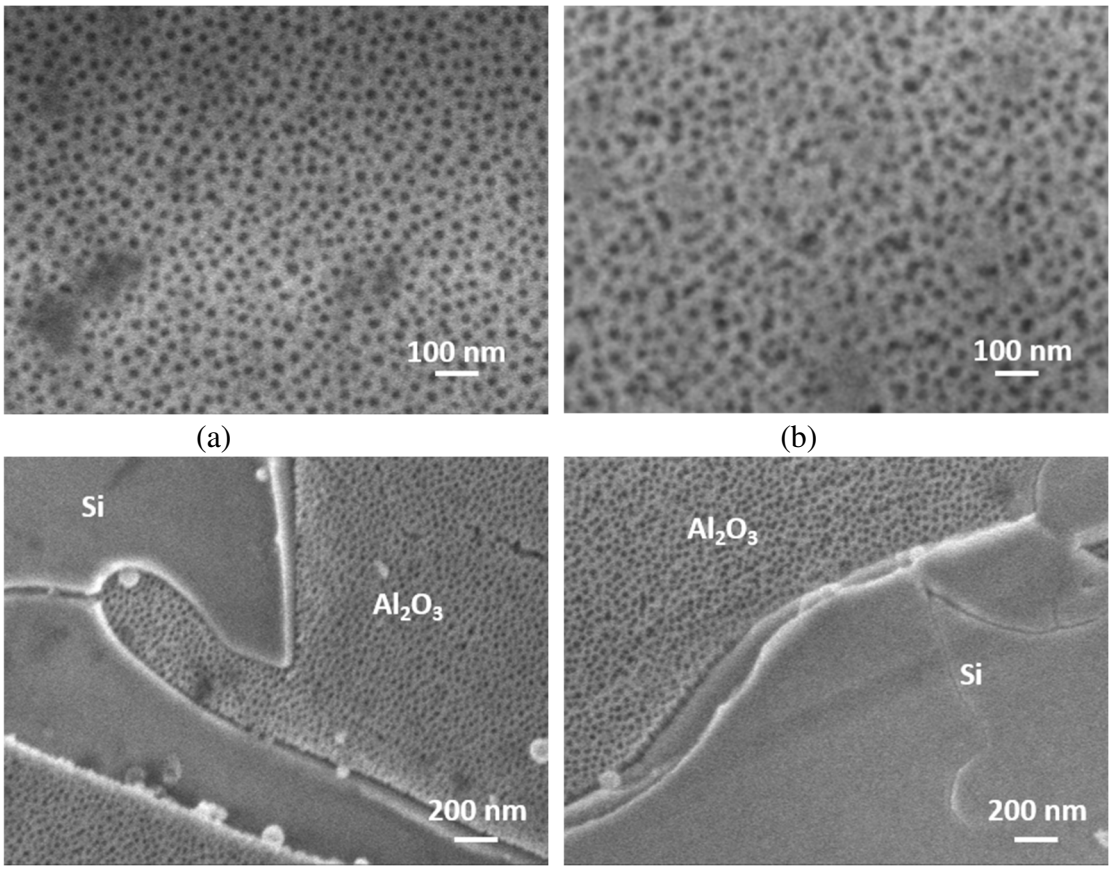


**Figure 3.** SEM surface observation (a) (c) after 90 min of sulfuric anodizing ($H_2SO_4$ 1 M, 15 V); (b) (d) followed by 15 min of impregnation in a sealing solution ($CH_3(CH_2)_8COONa$ 0.01 M, 50°C).

The electrochemical conditions to get a 15-µm thick coating in microarc oxidation differs from the conditions applied in sulfuric medium, since the electrochemical behaviour of the substrate in an alkaline medium is different (Figure 4a). Indeed, AS12 substrate exhibits a passivation/anodizing range until about 450 V with an anodic current density remaining relatively low over this large range thanks to a judicious choice of the electrolytic composition [44]. Therefore, the microarc oxidation regime may be reached since the

breakdown potential and the initiation of the sparks occurs around 350 V, namely the voltage of sparking initiation observed on pure aluminium. The formation of the microarc coating was then achieved by using a bipolar pulsed signal under current control in order to optimize the morphology [27, 49-50]. A typical part of the applied (current density) and recorded (voltage) electrical signals is represented in Figure 4b over 4 periods. During the anodic stages performed at +100 mA $cm^{-2}$, the voltage stabilizes around 500 V consistently with the potentiodynamic curve (Figure 4a), which induces the growth of an anodic layer under a microarc oxidation regime. Since the cathodic stages do not contribute directly to the formation of the anodic layer, they are not fundamentally investigated in the current paper via cathodic potentiodynamic scan. However, these cathodic stages are known to be crucial to favour a compact morphology of the anodic layer via various cathodic electrochemical mechanisms still in discussion in the literature [51].

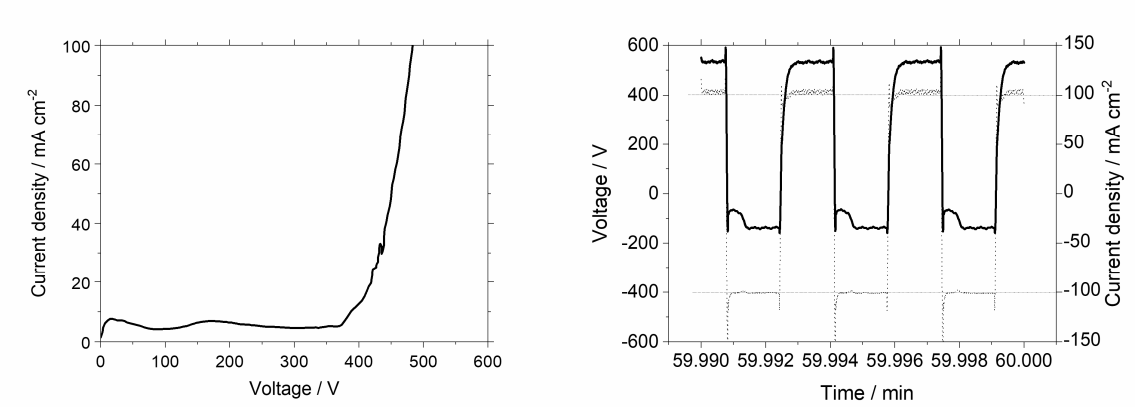


**Figure 4.** Electrochemical investigation of the microarc oxidation process (KOH 0.0025 M + $Na_2SiO_3$ 0.01 M + KF 0.001 M): (a) anodic potentiodynamic scan (10 V $min^{-1}$) over the range 0-500 V; (b) voltage over 4 periods during a microarc oxidation carried out with a pulsed signal (+ 100 mA $cm^{-2}$, 100 ms / - 100 mA $cm^{-2}$, 100 ms).

The growth rate of the anodic layer is constant with oxidation time, in the order of 2.1 µm $min^{-1}$ (Figure 5a). As referred elsewhere [30-33, 44], SEM cross section observations (Figure

5b) coupled with EDX punctual analyses have revealed that both the aluminium matrix and the silicon lamella embedded in the substrate are oxidized, respectively into alumina and silica in the inner part of the microarc layer, while the intermetallic particles are dealloyed and covered by alumina. From the morphological point of view, discharge channels, specific of the microarc process, are obvious through the layer viewed in cross-section (Figure 5b) and result in a typical island-like morphology in surface (Figure 6a). The corresponding micrometric holes in surface do not seem to be covered after impregnation in the sealing solution (Figure 6b).

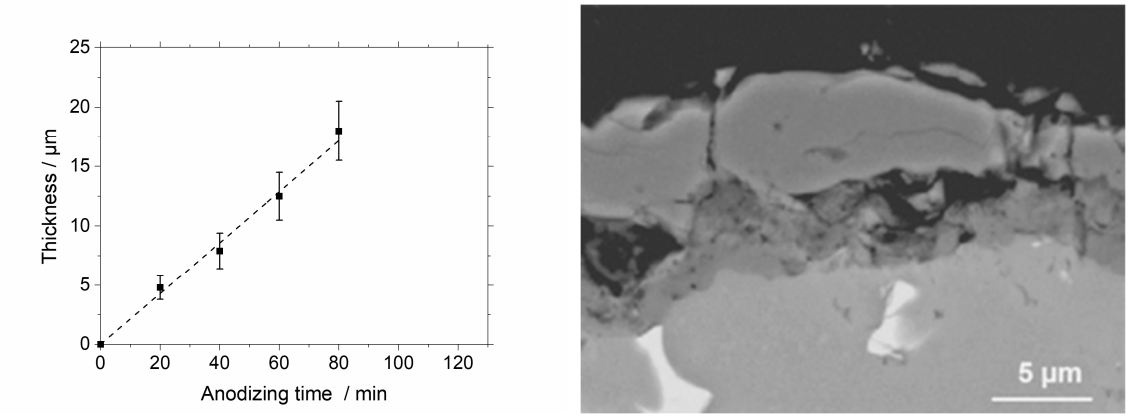


(a) (b)

**Figure 5.** (a) Growth kinetics of the anodic layer in KOH 0.0025 M + $Na_2SiO_3$ 0.01 M + KF 0.001 M with a pulsed signal (+ 100 mA $cm^{-2}$, 100 ms / - 100 mA $cm^{-2}$, 100 ms); (b) SEM cross-section observation after 70 min of microarc oxidation.

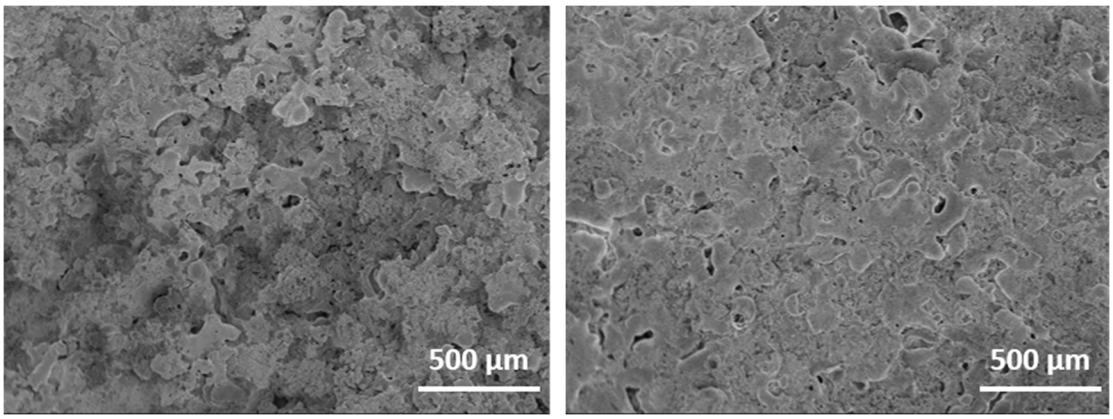

(a) (b)

**Figure 6.** SEM surface observation (a) after 70 min of microarc anodizing (KOH 0.0025 M + $Na_2SiO_3$ 0.01 M + KF 0.001 M, pulsed signal + 100 mA $cm^{-2}$, 100 ms / - 100 mA $cm^{-2}$, 100 ms); (b) followed by 15 min of impregnation in a sealing solution ($CH_3(CH_2)_8COONa$ 0.01 M, 50°C).

***Evaluation of the corrosion resistance***

The corrosion resistance of the alloys, treated either by sulfuric anodizing or microarc oxidation, followed or not by impregnation in sodium decanoate, is evaluated by EIS performed in NaCl 0.1 M (Figure 7) and by exposure to a neutral SST (Figure 8). All the results are compared with the behaviour of untreated samples.

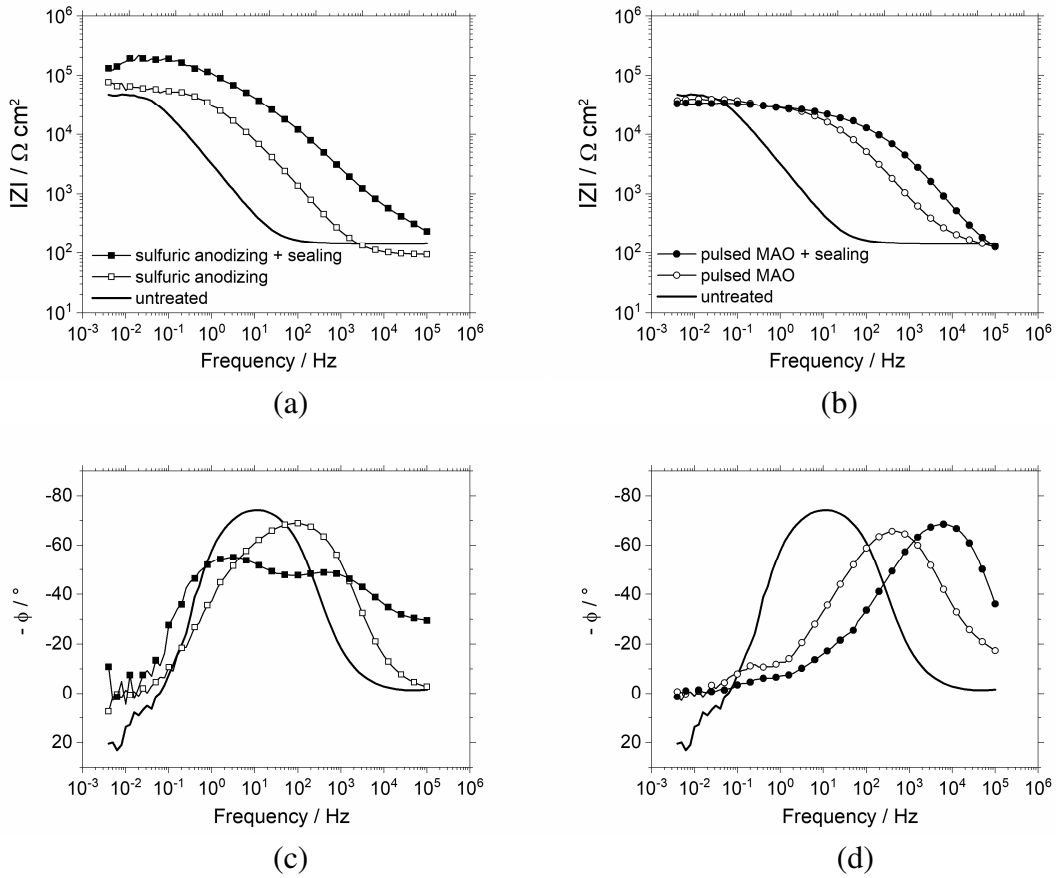


**Figure 7.** Bode representations ((a)(b) modulus ; (c)(d) phase) of the electrochemical impedance spectra recorded after 6 hours of immersion in NaCl 0.1 M on AS12 (a)(c) untreated, after 90 min of sulfuric anodizing ($H_2SO_4$ 1 M, 15 V), then 15 min of impregnation

in a sealing solution ($CH_3(CH_2)_8COONa$ 0.01 M, 50°C) ; (b)(d) untreated, after 70 min of microarc oxidation (KOH 0.0025 M + $Na_2SiO_3$ 0.01 M + KF 0.001 M, pulsed signal + 100 mA $cm^{-2}$, 100 ms / - 100 mA $cm^{-2}$, 100 ms), then 15 min of impregnation in a sealing solution ($CH_3(CH_2)_8COONa$ 0.01 M, 50°C).

Regarding the electrochemical results on the untreated sample (Figure 7), the recorded impedance spectra obviously exhibit one time-constant with a characteristic frequency around $10^1$ Hz, taking both the charge transfer resistance and the double layer capacitance at the electrolyte / substrate interface into account. Moreover, at frequencies lower than $10^{-1}$ Hz, the signal turns unstable (Figure 7c), which is likely correlated with a pitting phenomenon. Besides, the phase of the complex impedance gets a positive value, which may be attributed to the adsorption of ionic species overall the electroactive surface, for instance chloride anions which are involved in the pitting of aluminium alloys. In the case of treated samples, either by sulfuric anodizing (Figures 7a and Figure 7c) or microarc oxidation (Figure 7b and Figure 7d), the impedance spectra clearly show two time constants: one has a characteristic frequency in the range $10^3$-$10^4$ Hz, the second has a characteristic frequency in the range $10^{-1}$ – $10^0$. A special attention should be paid to the very low frequency range, especially on the impedance phases (Figures 7c and Figure 7d). Indeed, while the impedance phase remains noisy for the sample anodized in sulfuric acid (even after impregnation in the sealing solution), revealing a sensitivity to the pitting corrosion, the signal becomes smooth after microarc oxidation.

As indicated qualitatively by the electrochemical results (Figure 7) and confirmed by the observations made after exposure to SST (Figure 8), the main corrosion phenomena occurring in concentrated salty solutions are mainly localized which makes tricky any quantitative interpretation of the data by the means of an equivalent electrical model. Therefore, in order to compare the effect of the two treatments and highlight the potential impact of the sealing,

an improvement factor I has been defined [40], based on the damage factor described for protective coatings [52]. Actually, for a fixed frequency *f*, $I_f$ is defined by:

$$\mathbf{I}_f = \ log \ \frac{|\boldsymbol{Z}_{\mathbf{treated}}|_f}{|\boldsymbol{Z}_{\mathbf{untreated}}|_f}$$

where $|Z_{untreated}|_f$ corresponds to the impedance modulus recorded at the frequency *f* on the untreated AS12 alloy and $|Z_{treated}|_f$ corresponds to the impedance modulus recorded at the frequency *f* on a treated AS12 alloy, whatever the considered treatment: sulfuric anodizing, microarc oxidation, eventually followed by a sealing post-impregnation. In order to investigate qualitatively the corrosion resistance of the samples, two frequencies have been chosen as representative of the both electrochemical constants namely $10^3$ Hz and $10^{-2}$ Hz. The calculated improvement factors are gathered in the Table 2.

**Table 2.** Improvement factor I

| | **Sulfuric anodizing** | | **Pulsed MAO** | |
|---|---|---|---|---|
| | / | + sealing | / | + sealing |
| $I_{10^3Hz}$ | 0.2 | 1.3 | 0.8 | 1.4 |
| $I_{10^{-2}Hz}$ | 0.1 | 0.5 | -0.1 | -0.2 |

According to these values, sulfuric anodizing seems to have no meaningful influence on the impedance modulus recorded at $10^3$ or $10^{-2}$ Hz, while microarc oxidation significantly improves the value at $10^3$ Hz. The sealing even slightly enhances $I_{10^3Hz}$ after microarc oxidation but greatly increases $I_{10^3Hz}$ after sulfuric anodizing. Finally, $I_{10^3Hz}$ reaches the same level after oxide formation followed by sealing, whatever the treatment for oxide growth. Furthermore, $I_{10^{-2}Hz}$, unchanged after oxide formation by both treatments, is slightly enhanced by the sealing post-treatment only after sulfuric anodizing.

The electrochemical results described above (Figure 7, table 2) are compared with visual observations after accelerated corrosion tests performed in a salt spray chamber (Figure 8). As revealed in Figure $8a_1$, the untreated sample exhibits numerous and large corrosion marks

early, from 6 hours of exposure. The early start of the corrosion is obvious as well on the sample treated by sulfuric anodizing (Figure $8b_1$), with a generalized process overall the surface even if the corrosion marks remain smaller than on the untreated sample. Regarding the sample treated by microarc oxidation, it seems to be intact after 6 hours in the SST chamber (Figure $8c_1$). Actually, small and localized (but numerous) corrosion tracks finally appear, as revealed by the observation made after 240 hours of exposure to SST (Figure $8c_2$) but the level of attack remains largely reduced compared with the entire damage of the surface undergone by the untreated sample (Figure $8a_2$) and the anodized one (Figure $b_2$): in these two last cases, the all surface is covered by large corrosion marks. The post-impregnation in the sealing solution clearly brings a significant enhancement of the corrosion resistance of both samples covered by an anodic layer: the level of deterioration is greatly reduced on the sample anodized in sulfuric acid (Figure $8b_3$), and only a few pits remain on the surface treated by microarc oxidation followed by a sealing treatment (Figure $8c_3$).

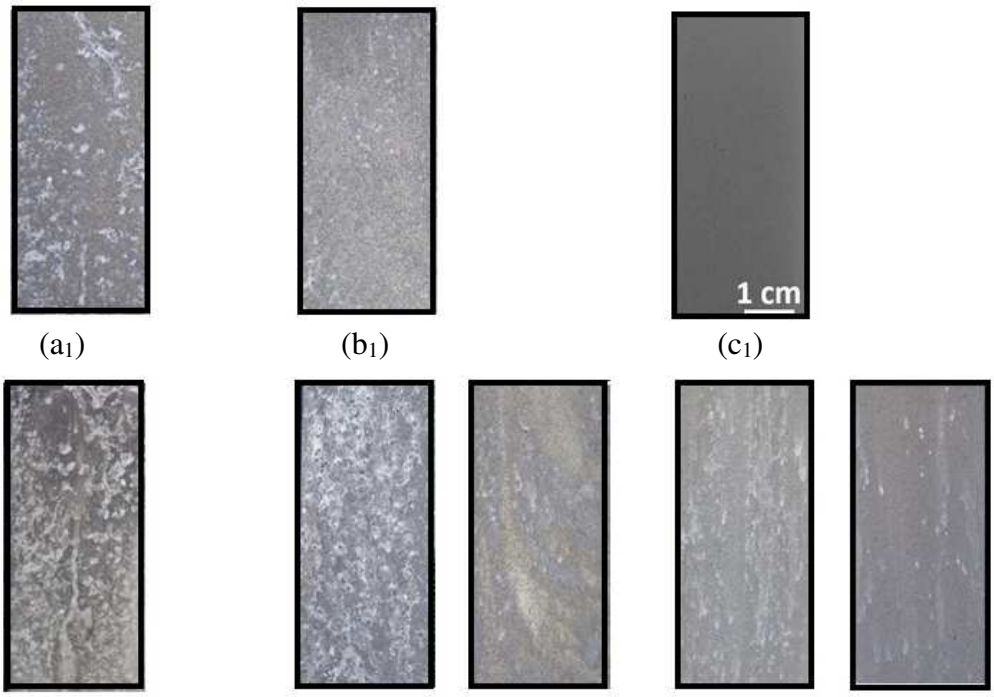

**Figure 8.** Visual observation of AS12 samples exposed to neutral SST: untreated after ($a_1$) 6 H; ($a_2$) 240 H ; anodized in sulfuric acid after ($b_1$) 6 H ; ($b_2$) 240 H ; (b3) anodized in sulfuric acid then impregnated in a sealing solution, after 240 H ; treated by microarc oxidation after ($c_1$) 6 H ; ($c_2$) 240 H ; (c3) treated by microarc oxidation then impregnated in a sealing solution, after 240 H.

The corrosion mechanims after 240 hours of exposure are highlighted at the microscopic level on cross sections (Figure 9). On the untreated sample (Figure 9a), the corrosion is characterized by the superficial oxidation of the substrate (left side of the picture), locally turning into the formation of a spherical pit (middle of the picture) with a depth in the range of 100 µm. The deposit of corrosion products is obvious outside the pit (right side of the picture). Actually, as revealed by the contrasts and confirmed by EDX punctual analyses, the corrosion of the substrate consists in the oxidation of the aluminium matrix while the numerous silicon lamella and the few intermetallic particles remain metallic. The corrosion process is then mainly driven by the galvanic coupling on the surface between the aluminium-rich matrix and silicon lamella. In the cases of samples initially covered by an anodic layer, either grown by anodizing in sulfuric acid (Figure 9b) or by microarc oxidation (Figure 9c), the initiation of the observed pits, underneath the 15 µm-thick coating, seems to be more localized than on the untreated sample. The resulting pits are therefore narrower on the surface. However, while the depth of the pits formed under the microarc coating (Figure 9c) seems to be reduced in comparison with the untreated sample, the pits formed under the anodic layer are very deep (Figure 9b), several hundreds of microns.

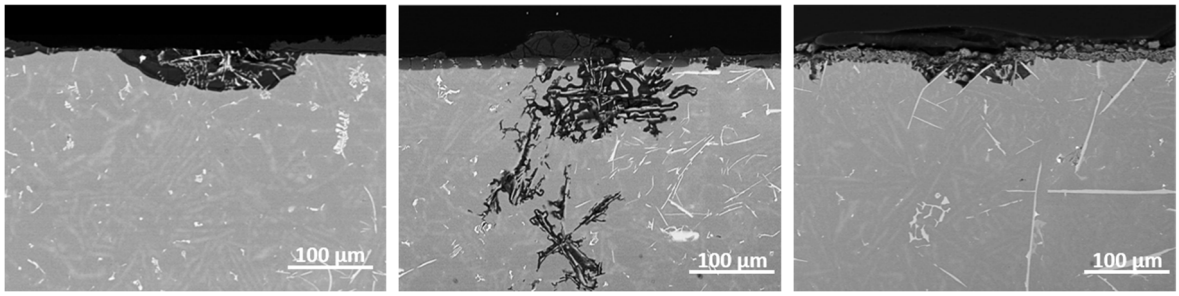

(a) (b) (c)

**Figure 9.** SEM cross section observation after 240 H of exposure to neutral SST of AS12 samples (a) untreated; (b) anodized in sulfuric acid ($H_2SO_4$ 1 M, 15 V, 90 min); (c) treated by microarc oxidation (KOH 0.0025 M + $Na_2SiO_3$ 0.01 M + KF 0.001 M, 70 min of pulsed signal + 100 mA $cm^{-2}$, 100 ms / - 100 mA $cm^{-2}$, 100 ms).

## 4. Discussion

Both sulfuric anodizing and microarc treatments applied to AS12 alloy lead to cracked anodic layers, with a main difference lying in the localization of defects. For sulfuric anodizing, the cracks are localized in the interspaces between alumina and silicon in the oxide or in the neighborhood of the silicon lamella, forming easy paths for the electrolyte from the outside environment to the substrate. In the case of microarc oxidation, some cracks cross the coating as well, due to the plasma discharges forming channels, exclusively localized over the aluminium matrix and not on the silicon phase [32]. The location of the cracks is then a key point regarding the corrosion resistance mechanism and performance. Actually, the main corrosion mechanism undergone by AS12 alloys is galvanic coupling between aluminium and silicon, inducing the preferential corrosion of aluminium around the silicon lamella. Therefore, in the case of sulfuric anodizing, since the access of the electrolyte to the substrate is mainly localized in the vicinity of silicon particles, the pitting initiation is promoted as it is consistently observed by early degradation in the salt spray chamber and by the noisy electrochemical impedance signal at very low frequencies. The number of pits initiated very early in the degradation process is very high as observed after only 6 hours of exposure to the salt spray chamber but, since the alumin~~a~~ium matrix is covered by the anodic layer, the pits do not extend over the surface and keep a limited diameter at the beginning of the process. However, this

surface confinement hides a very high activity in the depth and the propagation of the pits towards the substrate core is much more severe underneath the sulfuric anodized coatings than under the untreated surface, as revealed by the cross sections realized after the accelerated degradation in the salt spray chamber. Regarding microarc oxidation, thanks to the localization of the discharge channels only over the aluminium matrix, the galvanic coupling is greatly avoided. This results in a large reduction of the pits when the sample are exposed to the salt spray chamber. Finally, by considering only corrosion properties, microarc oxidation carried out in alkaline medium provides a better resistance than sulfuric anodizing, without any sealing post-treatment. However, not only the corrosion resistance needs to be considered. Further properties such as wear reinforcement for instance (provided by the formation of ceramic-like phases under the effect of sparks), suitability for further paint treatment, as well as process consideration such energetic consumption, toxicity of the electrolytic bath, may guide the final choice in a global lifecycle assessment.

For both oxide layers, the post-impregnation in the sodium decanoate solution has a beneficial effect, more significant on samples anodized in sulfuric acid. In the case of long-chain carboxylates used in sealing solutions for porous alumina layers, the main reaction involved is the adsorption of the carboxylates on the alumina surface. Then, two aspects must be considered: the binding energy within the formed surface complex, related to the affinity between the decanoate and the compounds in surface, as well as the limitation of the ionic diffusion in the porosities governed their size and morphology. Actually, the alumina walls formed in sulfuric acid are positively charged and sulfates are adsorbed. The binding energy being stronger between alumina and carboxylates than between alumina and sulfates, a desorption/readsorption mechanism occurs during the sealing treatment leading to the formation of stable complexes on the surface of alumina. The carboxylates may adsorb on silicon nanopoarticles as well. Ceramic alumina (and aluminosilicates) formed by microarc

oxidation is less reactive and the adsorption of carboxylates in surface is less favoured. Moreover, since the electrolytic paths between the nanoporous alumina and the silicon nanoparticles resulting from sulfuric anodizing, are thinner than the discharge channels created by microarc oxidation, the diffusion limitation thanks to the formed hydrophobic complex is more efficient after the sealing of layer grown by sulfuric anodizing.

For such defective anodic layer and such localized corrosion phenomena mainly driven by galvanic coupling under the anodic layer, the exploitation of the EIS results remains tricky and providing mechanistic interpretations is hazardous. However, based on the comparison between EIS measurements and observations after exposure in the salt spray chamber of the different configurations investigated in the present paper, it seems that the value of the impedance modulus in the middle range of frequency (more specifically, its enhancement regarding an untreated sample) represents a more reliable indicator of the pitting corrosion resistance than the impedance modulus at low frequency which is usually used for estimating the barrier efficiency of organic coatings.

## 5. Conclusion

The corrosion sensitivity of AS12 alloys is mainly driven by the galvanic coupling between the α-aluminium matrix and the silicon lamella dispersed within. Usual protection brought to aluminum alloys by sulfuric anodizing is not efficient since preferential electrolytic paths are created in the coating in the interspaces between alumina and silicon remaining under metallic form. Instead, the corrosion resistance may be largely enhanced by microarc oxidation. The post-impregnation of the coated materials in a sodium decanoate sealing solution shows a real improvement in both cases and the corrosion marks may even be limited to a few pits after 240 hours of SST when post-impregnation is performed after microarc oxidation of AS12 substrate.

**Acknowledgement**

This work was financially supported by the "PHC Utique" program of the French Ministry of Foreign Affairs and Ministry of higher education, research and innovation and the Tunisian Ministry of higher education and scientific research in the CMCU project number 18G1140.

**References**

[1] G.E. Thompson, Porous anodic alumina: fabrication, characterization and applications, Thin Solid Films 297 (1997) 192-201.

[2] L. Zhang, G.E. Thompson, M. Curioni, P. Skeldon, Anodizing of aluminum in sulfuric acid / boric acid mixed electrolyte, Journal of the Electrochemical Society, 160 (2013) C179-C184.

[3] M. Curioni, T. Gionfini, A. Vicenzo, P. Skeldon, G.E. Thompson, Optimization of anodizing cycles for enhanced performance, Surface and Interface Analysis 45 (2013) 1485-1489.

[4] T. Aerts, Th. Dimogerontakis, I. De Graeve, J. Fransaer, H. Terryn, Influence of the anodizing temperature on the porosity and the mechanical properties of the porous anodic film, Surface and Coatings Technology 201 (2007) 7310-7317.

[5] N. Tsyntsaru, B. Kavas, J. Sort, M. Urgen, J.P. Celis, Mechanical and frictional behavior of nanoporous anodized aluminum, Materials Chemistry and Physics 148 (2014) 887-895.

[6] J. V.de Sousa Araujo, M. Milagre, I. Costa, A historical, statistical and electrochemical approach on the effect of microstructure in the anodizing of Al alloys: a review, Critical Reviews in Solid State and Materials Sciences 49 (2024) 521-581.

[7] S.J. Garcia-Vergara, K. El Khazmi, P. Skeldon, G.E. Thompson, Influence of copper on the moprhology of porous anodic alumina, Corrosion Science 48 (2006) 2937-2946.

[8] I. Tsangaraki-Kaplanoglou, S. Theohari, T. Dimogeontakis, Y.M. Wang, H.H. Kuo, S. Kia, Effect of alloy types on the anodizing process of aluminum, Surface and Coatings Technology 200 (2006) 2634-2641.

[9] L. Iglesias-Rubianes, S.J. Garcia-Vergara, P. Skeldon, G.E. Thompson, J. Ferguson, M. Beneke, Cyclic oxidation processes during anodizing of Al-Cu alloys, Electrochimica Acta 52 (2007) 7148-7157.

[10] M. Saenz de Miera, M. Curioni, P. Skeldon, G.E. Thompson, Modelling the anodizing behaviour of aluminium alloys in sulphuric acid through alloy analogues, Corrosion Science 50 (2008) 3410-3415.

[11] Y. Ma, X. Zhou, G.E. Thompson, M. Curioni, X. Zhong, E. Koroleva, P. Skeldon, G.E. Thompson, M. Fowles, Discontinuities in the porous anodic film formed on AA2099-T8 aluminium alloy, Corrosion Science 53 (2011) 4141-4151.

[12] B. Mazurkiewicz, A. Piotrowski, The electrochemical behaviour of $Al_2Cu$ intermetallic compound, Corrosion Science 23 (1983) 697-707.

[13] R.G. Buchheit, R.P. Grant, P.F. Hlava, B. Mckenzie, G.L. Gender, Local dissolution phenomena associated with S phase ($Al_2CuMg$) particles in aluminium alloy 2024-T3, Journal of the Electrochemical Society 144 (1997) 2621-2628.

[14] K. Shimizu, K. Kobayashi, G.E. Thompson, P. Skeldon, G.C. Wood, The influence of θ' precipitates on the anodizing behaviour of binary Al-Cu alloys, Corrosion Science 39 (1997) 281-284.

[15] M. Saenz de Miera, M. Curioni, P. Skeldon, G.E. Thompson, Preferential anodic oxidation of second-phase constituents during anodizing of AA2024-T3 and AA7075-T6 alloys, Surface and Interface Analysis 42 (2010) 241-246.

[16] M. Saenz de Miera, M. Curioni, P. Skeldon, G.E. Thompson, The behaviour of second phase particles during anodizing of aluminium alloys, Corrosion Science 52 (2010) 2489-2497.

[17] L.E. Fratila-Apachitei, J. Duszczyk, L. Katgerman, Al(Si)Cu anodic oxide layers formed in $H_2SO_4$ at low temperature using different current waveforms, Surface and Coatings Technology 165 (2003) 232-240.

[18] O.O. Knudsen, B.S. Tanem, A. Bjorgum, J. Mardalen, M. Hallenstvet, Anodising as pretreatment before organic coating of extruded and cast aluminium alloys, Corrosion Science 46 (2004) 2081-2095.

[19] A. Forn, J.A. Picas, M.T. Bale, E. Martin, V.G. Garcia, Microstructure and tribological properties of anodic oxide layer formed on Al-Si alloy produced by semi-solid processing, Surface and Coatings Technology 202 (2007) 1139-1143.

[20] R.I. Revilla, H. Terryn, I. De Graeve, Role of Si in the Anodizing Behavior of Al-Si Alloys: Additive Manufactured and Cast Al-Si10-Mg. Journal of the Electrochemical Society 165 (2018) C532-C541.

[21] R.I. Revilla, Y. Rojas, I. De Graeve On the Impact of Si Content and Porosity Artifacts on the Anodizing Behavior of Additive Manufactured Al-Si Alloys, Journal of the Electrochemical Society 166 (2019) C530-C537.

[22] D. Veys-Renaux, E. Rocca, Initial stages of multi-phased aluminium alloys anodizing by MAO: micro-arc conditions and electrochemical behavior, Journal of Solid State Electrochemistry 19 (2015) 3121-3129.

[23] S. Ikonopisov, Theory of electrical breakdown during formation of barrier anodic films, Electrochimica Acta 22 (1977) 1077-1082.

[24] A.L. Yerokhin, X. Nie, A. Leyland, A. Matthews, S.J. Dowey, Plasma electrolysis for surface engineering, Surface and Coatings Technology122 (1999) 73-93.

[25] A.L. Yerokhin, V.V. Lyubimov, R.V. Ashitkov, Phase formation in ceramics coatings during plasma electrolytic oxidation of aluminium alloys, Ceramics International 24 (1998) 1-6.

[26] F. Monfort, A. Berkani, E. Matykina, P. Skeldon, G.E. Thompson, H. Habazaki, K. Shimizu, Development of anodic coatings on aluminium under sparking conditions in silicate electrolyte, Corrosion Science 49 (2007) 672-693.

[27] R.H.U. Khan, A. Yerokhin, X. Li, H. Dong, A. Matthews, Surface characterization of DC plasma electrolytic oxidation treated 6082 aluminium alloy: Effect of current density and electrolyte concentration, Surface and Coatings Technology 205 (2010) 1679-1688.

[28] Lei Wen, Yaming Wang, Yu Zhou, Jia-Hu Ouyang, LixinGuo, DechangJia, Corrosion evaluation of microarc oxidation coatings formed on 2024 aluminium alloys, Corrosion Science 52 (2010) 2687-2696.

[29] R.F. Zhang, H.W. Shi, Z. Liu, S.F. Zhang, Y.Q. Zhang, S.B. Guo, Properties of anodic coatings obtained in an organic, environmental friendly electrolyte on aluminium alloy 2024-T3, Applied Surface Science 289 (2014) 326-331.

[30] F. Xu, Y. Xia, G. Li, The mechanism of PEO process on Al–Si alloys with the bulk primary silicon, Applied Surface Science 255 (2009) 9531–9538.

[31] J. He, Q.Z. Cai, H.H. Luo, L Yu, B.K. Wei, Influence of silicon refinement on growth process of plasma electrolytic coating on Al-Si alloy, Journal of Alloys and Compounds 471 (2009) 395-399.

[32] K. Li, W. Li, G. Zhang, W. Zhu, F. Zheng, D. Zhang, M. Wang, Effects of Si phase refinement on the plasma electrolytic oxidation of eutectic Al-Si alloy, Journal of Alloys and Compounds 790 (2019) 650-656.

[33] A. B. Rogov, H. Lyu, A. Matthews, A.Yerokhin, AC plasma electrolytic oxidation of manufactured and cast AlSi12 alloys, Surface and Coatings Technology 399 (2020) 126116.

[34] L. Hao, B. R. Cheng, Sealing processes of anodic coatings—past, present, and future, Metal Finishing 98 (2000) 8-18.

[35] K. Bonnel, C. Le Pen and N. Pébère, E.I.S. characterization of protective coatings on aluminum alloys, Electrochimica Acta 44 (1999) 4259-4267.

[36] M. Mohedano, E. Matykina, R. Arrabal, B. Mingo, A. Pardo, PEO of pre-anodized Al–Si alloys: Corrosion properties and influence of sealings, Applied Surface Science 346 (2015) 57–67.

[37] M. R. Kalantary, D. R. Gabe, et D. H. Ross, A model for the mechanism of nickel fluoride cold sealing of anodized aluminium, Journal of Applied Electrochemistry 22 (1992) 268–276.

[38] F. Mansfeld, C. Chen, C. B. Breslin, D. Dull., Sealing of anodized aluminum alloys with rare earth metal salt solutions, Journal of The Electrochemical Society 145 (1998) 2792-2798.

[39] R. Gaggiano, P. Moriamé, M. Biesemans, I. De Graeve, H. Terryn, Mechanism of formation of silicate thin films on porous anodic alumina, Surface and Coatings Technology 205 (2011) 5210–5217.

[40] N. Chahboun, E. Rocca, D. Veys-Renaux, M. Augros, M. Boutoba, N. Caldeira, Sealing of anodized multiphase aluminium alloys with Cr(+III)/Zr(+IV) salts: characterization and corrosion behaviour, Journal of the Electrochemical Society (2016) C1-C7.

[41] N. Chahboun, D. Veys-Renaux, E. Rocca, Impregnation of nanoporous alumina in a fluorozirconate salt containing solution, Applied Surface Science 541 (2021) 148459.

[42] G. P. Shulman, A. J. Bauman, Corrosion Protection with Organic Acid Sealants for Anodized Aluminum, Journal of The American Chemical Society 689 (1998) 420-422.

[43] G. Boisier, N. Portail, N. Pébère, Corrosion inhibition of 2024 aluminium alloy by sodium decanoate, Electrochimica Acta 55 (2010) 6182-6189.

[44] A. BenRomdhane, D. Veys-Renaux, M.M. Ndiaye, S. Bruyère, K. Elleuch, E. Rocca, Anodizing of AS12 alloy in alkaline media, Applied Surface Science 572 (2022) 151436.

[45] J.G. Barlock, L.F. Mondolfo, Structure of some aluminium iron manganese silicon alloys, Zeitschrift für Metalkunde 66 (1975) 605-611.

[46] D. Veys-Renaux, N. Chahboun, E. Rocca, Anodizing of multiphase aluminium alloys in sulfuric acid: in situ electrochemical behaviour and oxide properties, Electrochimica Acta 211 (2016) 1056-1065.

[47] A. Gasco-Owens, D. Veys-Renaux, V. Cartigny, E. Rocca, Large-pores anodizing of 5657 aluminum alloy in phosphoric acid: an in-situ electrochemical study, Electrochimica Acta 382 (2021) 138303.

[48] L. Arurault, Pilling–Bedworth ratio of thick anodic aluminium porous films prepared at high voltages in $H_2SO_4$ based electrolyte. Transactions of the Institute of Metal Finishing 86 (2008) 51- 54.

[49] F. Jaspard-Mécuson, T. Czerwiec, G. Henrion, T. Belmonte, L. Dujardin, A. Viola, J. Beauvir, Tailored aluminium oxide layers by bipolar current adjustment in the Plasma Electrolytic Oxidation (PEO) proces*s*, Surface and Coatings Technology 201 (2007) 8677-8682.

[50] J. Martin, A. Melhem, I. Schedrina, T. Duchanoy, A. Nominé, G. Henrion, T. Czerwiec, T. Belmonte, Effects of electrical parameters on plasma electrolytic oxidation of aluminium, Surface and Coatings Technology 221 (2013) 70-76.

[51] A. Rogov, A. Yerokhin, A. Matthews, The role of cathodic current in plasma electrolytic oxidation of aluminium: phenomenological concepts of the “soft sparking” mode, Langmuir 33 (2017) 11059-11069.

[52] F. Mansfeld, M. W. Kendig, Electrochemical impedance spectroscopy of protective coatings, Materials and Corrosion 36 (1985) 473-483.